J Sol-Gel Sci Technol (2018) 85:302–310
DOI 10.1007/s10971-017-4553-2

ORIGINAL PAPER: FUNDAMENTALS OF SOL-GEL AND HYBRID MATERIALS PROCESSING

Role of oxalic acid in structural formation of sodium silicate-based silica aerogel by ambient pressure drying

Ha-Yoon Nah[1] · Vinayak G. Parale[1] · Hae-Noo-Ree Jung[1] · Kyu-Yeon Lee[1] · Chang-Hyun Lim[2] · Yang Seo Ku[3] · Hyung-Ho Park[1]

Received: 4 September 2017 / Accepted: 22 November 2017 / Published online: 30 November 2017

Abstract Recently, the demand of sodium silicate-based silica aerogels has decreased due to its inadequate physical properties when compared to those made by other silicon alkoxides. To avoid this problem, introduction of a drying control chemical additive (DCCA) in the sol has received great attention. DCCA is one of the additives that can control the rate of hydrolysis and the condensation reaction in sol state by the formation of hydrogen bonds between DCCA and silanol groups of silica sol. A control over these reactions results in a uniform pore size distribution, which, in turn, decreases the drying stress with a decrease in pore size, in accordance with the Young–Laplace equation. Therefore, the structure of the silica aerogel can be maintained by minimizing the volume shrinkage due to drying stress. In this research, oxalic acid was first used as DCCA in the formation of sodium silicate-based silica aerogel by ambient pressure drying. The physical properties of these silica aerogels can be changed by changing the molar ratio of oxalic acid/Na_2SiO_3 in the sol state. When the oxalic acid:Na_2SiO_3 molar ratio was 15×10^{-4} in the sol state, aerogels with high specific surface area (623.2 m^2/g), pore volume (4.271 cm^3/g), average pore diameter (27.41 nm), high porosity (94.3%), high contact angle (144.09°), and high optical transmittance (75%) were obtained.

Graphical abstract

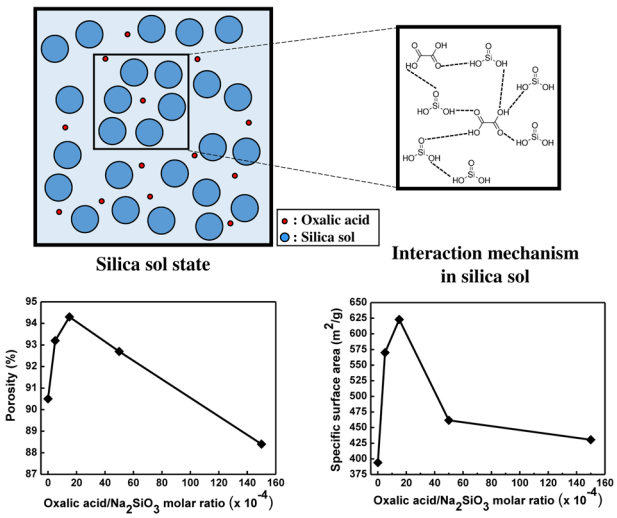

Keywords Sodium silicate · Silica aerogel · Ambient pressure drying · Drying control chemical additive · Oxalic acid

1 Introduction

An aerogel is usually synthesized by the sol–gel process and has received attention as a prospective material for various

Electronic supplementary material The online version of this article (https://doi.org/10.1007/s10971-017-4553-2) contains supplementary material, which is available to authorized users.

✉ Hyung-Ho Park
hhpark@yonsei.ac.kr

[1] Department of Materials Science and Engineering, Yonsei University, 50 Yonsei-ro, Seodaemun-gu, Seoul 03722, South Korea

[2] Korea Institute of Ceramic Engineering and Technology, 101 Soho-ro, Jinju-si, Gyeongsangnam-do 52851, South Korea

[3] GLChem Co., Ltd., 143 Yeocheon 3-gil, Ochang-eup, Cheongwon-gu, Cheongju-si, Chungcheongbuk-do 28127, South Korea

applications after Kistler developed it in 1931 [1]. It has various interesting physical characteristics such as high porosity (>90%), low density (~0.08 g/cm^3), and low thermal conductivity (15 mW/m• K) [2]. Because of these unique properties, it can be applied extensively in various fields such as drug carrier, oil absorber, gas storage, sensor, aerospace, sound insulation, heat insulator, hydrogen storage media, capacitor, battery, dielectric substances, and filters [1–4]. There are various kinds of the aerogels such as silica [4], resorcinol-formaldehyde [5], polymer [6], tin oxide [7], and zinc oxide [8]. Among these, silica aerogels have been extensively studied and informative results have been published.

Generally, the two types of silica aerogel precursors primarily used for preparation are silicon alkoxide and sodium silicate [9]. The silica aerogels synthesized by silicon alkoxides show better properties than those synthesized by sodium silicate precursor (also known as water-glass). However, the cost of silicon alkoxides poses a major barrier for the commercialization of silica aerogels [10]. In contrast, sodium silicate-based silica aerogel has poor physical properties, which is the main drawback of sodium silicate as a precursor for silica aerogel [11]. Therefore, researches have attempted to change the physical properties of sodium silicate-based silica aerogel by using tartaric acid [12]. Synthesis of superhydrophobic silica aerogel powder using sodium silicate via ambient pressure drying was developed by Bhagat et al. [13]. Toward this end, different strategies for the synthesis of sodium silicate-based silica aerogel have been reported [14–16]. The drying method for synthesizing the silica wet-gel can be divided into two different techniques: supercritical drying and ambient pressure drying. In the supercritical drying method, the solvent is transformed to a supercritical fluid during drying, which has zero surface tension that prevents the shrinkage and maintains the high porosity of the aerogel. However, the instrument used for supercritical drying is expensive, and drying conditions of high pressure and temperature are dangerous. In contrast, for ambient pressure drying, a surface modification agent was used on the silica wet-gel before the drying step in order to increase the shrinkage of aerogels and maintain the pore structure. Although the porosity and physical properties of ambient-dried aerogels are lower than those of supercritical dried aerogels, ambient pressure drying has major advantages over the supercritical drying method. The former requires ambient pressure with a relatively low temperature, and it is also safer and cheaper than the latter [16–18].

There are various reports on the effects of various factors on the synthesis of silica aerogel, such as molar ratio of the precursor and water [18], temperature [19], base and acid catalyst for hydrolysis, and condensation [19, 20]. The optimization of certain other parameters also led to the formation of silica aerogels with excellent physical properties. Some methods for improving the physical properties of silica aerogel by using co-precursors [21] and making composites [22] have also been reported. In these reports, the drying control chemical additive (DCCA) has received much more attention than others because it can prevent shrinkage by minimizing the drying stress [23]. Rao et al. have studied the effects of DCCA on silica aerogels dried by the supercritical drying method [24]. They found that the addition of glycerol to the sol affects the physical properties of the silica aerogel [25]. Some researchers have also reported the effect of N,N-dimethylformamide (DMF) as DCCA on silica aerogels [26]. Also, a report on advancing the properties of silica gel with the controlled rate of hydrolysis and condensation to form homogeneous silica alcogel is available [27]. This alcogel was converted into silica aerogels by using ambient pressure drying, which showed comparable changes in its physical properties. Till date, the effects of DCCA on trimethylorthosilicate and tetraethylorthosilicate-based silica aerogels have been reported [24, 28]. In contrast, there are insufficient reports on the effect of DCCA on water-glass-based aerogels. One group has reported the effects of glycerol [29] and DMF on sodium silicate-based silica aerogels [28]. In this work, oxalic acid was selected as the DCCA that is unique for solid-type, unlike other liquid-type DCCAs [24–29]. Here, the effect of oxalic acid on sodium silicate-based silica aerogel was investigated. This study provides more insights for analyzing the structural changes and physical properties based on the amount of oxalic acid used.

2 Experimental procedure

Sodium silicate-based silica aerogels with varying DCCA concentrations were synthesized by two-step sol–gel process, followed by ambient pressure drying method [30]. Sodium silicate solution (53 wt%, Duksan Chemical Co. Ltd., South Korea) was chosen as the precursor. The aging solvents were methanol (99.8%, Duksan Chemical Co. Ltd., South Korea) and n-hexane (95.0%, Duksan Chemical Co. Ltd., South Korea). Surface modification was carried out by using trimethylchlorosilane (TMCS; 98.0%, Daejung Chemicals & Metals Co., Ltd., South Korea). HCl (35%, Daejung Chemicals & Metals Co., Ltd., South Korea) was used as the acid catalyst and NH_4F (≥98.0%, Sigma-Aldrich, USA) was used as the base catalyst. They were used for hydrolysis and condensation of sodium silicate. Oxalic acid (≥99.0%, Sigma-Aldrich, USA) as DCCA was introduced as a solution. The molar ratio of oxalic acid/Na_2SiO_3 was varied from 0 to 150×10^{-4}. The amount of oxalic acid used did not affect the pH of silica sol, as its amount was much less than Na_2SiO_3. The sodium silicate solution with a

specific gravity of 1.05 was prepared by mixing sodium silicate and distilled water, and stirred at a speed of 300 rpm for 1 h. The solution pH was maintained around ~12. Sodium silicate should be completely dissolved in solution by stirring with a magnetic bar before starting hydrolysis. Then, the solution was stirred to form a homogeneous sol of sodium silicate by adding the catalyst and it was kept at room temperature for 4 h in order to promote hydrolysis by adding NH_4F solution as a catalyst. It leads to the formation of silicic acid from sodium silicate, and NaF was formed as byproduct or salt during the hydrolysis step. After the addition of NH_4F solution, oxalic acid solution was added as the DCCA while maintaining the pH and volume of the gel, and various samples of different concentrations and small volumes were synthesized. To avoid the effects of volume change, the volume percentage of oxalic acid solution was not allowed to exceed over 6% of the total hydrosol volume. The oxalic acid solution was made beforehand with molar concentrations of 0.001 M, 0.01 M, and 0.1 M, and introduced in silica sol by ball dropping method when required. The molar ratio of oxalic acid/Na_2SiO_3 were varied as 0, 5×10^{-4}, 15×10^{-4}, 50×10^{-4}, and 150×10^{-4} and named as A0, A1, A2, A3, and A4, respectively. After the hydrolysis step, hydrochloric acid solution was added for accelerating the condensation reaction. The molar ratio of Na_2SiO_3:H_2O:NH_4F:HCl was kept constant at 1:121.67:0.2467:4.144. After gelation, the gel was aged for 3 h in oven at 50 °C. It helps in the condensation reaction of Si–OH on the wet-gel surface and makes a large and thick skeleton. Thus, mechanical strength of the wet-gel becomes high at macro-scale [17]. Next, the gel was cut to obtain small granules and washed four times with deionized water, and solvent exchanged by methanol at 50 °C for 24 h. Surface modification was carried out by adding alcogels in a mixture of methanol, n-hexane, and TMCS with a constant volume ratio of 1:1:1. The reactor was sealed for surface modification at 50 °C in an oven for 24 h to float the gel on the surface. After that, wet-gels were washed with n-hexane for four times to remove any residue. The gel was aged using excess n-hexane at 50 °C in an oven for 24 h in order to strengthen the network. Finally, the modified wet-gels were dried at 50 °C for 1 h and at 200 °C for 1 h successively. The summary for this experimental process is presented as a flow chart in Fig. 1.

The bulk density was calculated using the mass to volume ratio. The volume was determined from a cylindrical column of a specific volume, which was filled with aerogel powders [31, 32], and the mass was measured by electronic microbalance with an accuracy of 10^{-5} g [30–32]. In addition, porosity of the samples was calculated by using the formula given below:

$$\text{Porosity} = (1 - \rho_b/\rho_s) \times 100(\%), \quad (1)$$

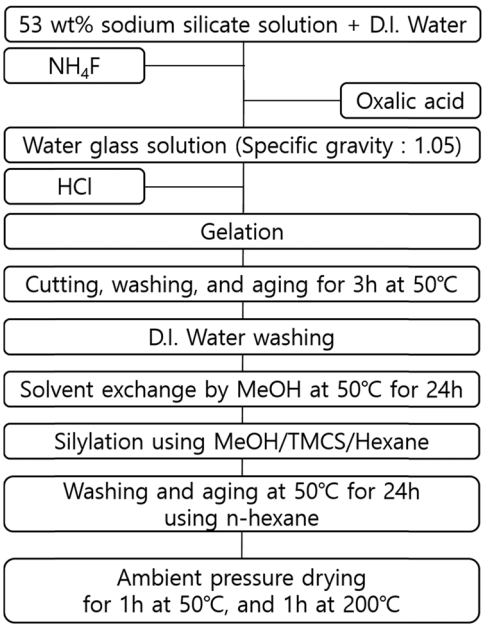

Fig. 1 Flow chart of the synthesis of water-glass-based silica aerogel

where ρ_b is bulk density and ρ_s is skeletal density of each sample. The ρ_s value was measured by using a helium pycnometer (Micromeritics, AccuPyc 1330, USA). The skeletal density values for all samples are ~1.8 g/cm^3. The chemical bonds in the water-glass-based silica aerogels were detected by Fourier transform infrared (FTIR) spectroscopy (Perkin Elmer, Model No. 760, USA) from wavenumbers 4000–400 cm^{-1}. The contact angle (θ) was measured by a contact angle meter (GITsoft, UNI-CAM-M-Dimension, South Korea) for analyzing the degree of hydrophobicity of the samples. The specific surface area was measured by Brunauer–Emmett–Teller (BET) analysis using the amount of N_2 gas adsorbed with the relative pressure in the range of $0.01 < P/P_0 < 1$, while the total pore volume, average pore diameter, and distribution of pore size were analyzed by the Barrett–Joyner–Halenda (BJH) method using a BET surface analyzer (Quantachrome, Autosorb-iQ, USA). The optical transmittance of each as-prepared aerogel granule was measured in triplicate by using a UV-visible spectrophotometer (JASCO, V-570, USA). The average size of the granules was around 2 mm, and the thickness of the cell used was 10 mm (Cuvets Quartz glass precision cell; Hellma, 6040-UV, Germany) in the wavelength range of 200–800 nm. A field-emission scanning electron microscope (FE-SEM; Carl Zeiss, Supra 40 VP, Germany) was used to investigate the microstructure of sodium silicate-based silica aerogels. Mechanical properties such as hardness and elastic modulus were measured by Nano Indentation at three different points (MTS, Nano Indenter XP, USA).

3 Results and discussion

The reported silica aerogels are prepared by two-step acid-base-catalyzed sol–gel process. The reaction mechanism under the synthesis conditions is explained through Eqs. (2) and (3).

$$\text{Hydrolysis: } Na_2SiO_3 + H_2O + 2NH_4F \rightarrow \equiv Si - OH + 2NaF + 2NH_3 \quad (2)$$

$$\text{Condensation: } \equiv Si - OH + HO - Si \equiv \rightarrow \equiv Si - O - Si \equiv + H_2O \quad (3)$$

It was observed that physical properties such as specific surface area, total pore volume, and average pore diameter improved when the reaction rate was appropriately controlled [24]. The maximum porosity observed for sample A2 was explained by controlling the hydrolysis and rate of condensation harmonically at the oxalic acid/Na_2SiO_3 molar ratio of 15×10^{-4} (sample A2). Since gelation was homogeneous, it led to a unique pore size distribution in most of the parts of water-glass sol. The porosity decreased with a further increase in the oxalic acid concentration, as the oxalic acid accelerates the condensation reaction in sol. Hence, a decrease in the homogeneous pore size is observed according to the Young–Laplace equation [12] when the drying stress is considered.

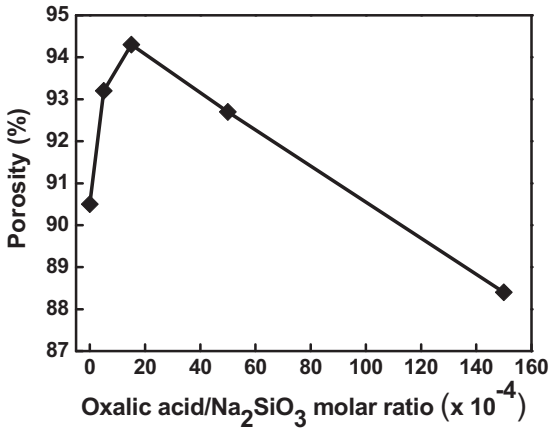

Fig. 2 Porosity as a function of oxalic acid/Na_2SiO_3 molar ratio

$$P = \frac{2\gamma\cos\theta}{r}, \quad (4)$$

where P is the capillary pressure, r is the pore radius, γ is the surface tension between liquid and pore wall, and θ is the contact angle at wetting condition. Equation (4) shows that the pore radius of the gel can affect the porosity of the final product as the capillary pressure and porosity are inversely proportional. Thus, the difference in the capillary pressure is smaller when the pore size is similar. Furthermore pore shrinkage was decreased and the porosity was increased. The change in porosity with various molar ratios of oxalic acid/Na_2SiO_3 is given in Fig. 2.

The information about the BET and BJH results of the prepared samples with varying oxalic acid/Na_2SiO_3 molar ratios is given in Table 1. It is confirmed that the specific surface area varies with the change in the concentration of oxalic acid. Figure 3 presents N_2 adsorption-desorption profiles for all prepared aerogel samples. Sample A2, which has the optimized concentration of oxalic acid, has the highest specific surface area. All graphs showed type IV isotherm with an H3 hysteresis loop, which confirmed the presence of mesopores and macropores in the prepared aerogels [26, 33]. An increase in the specific surface area was observed with increase in the oxalic acid/Na_2SiO_3 molar ratio. The highest specific surface area was observed for sample A2, as shown in Fig. 3. The specific surface area decreases with further increase in the concentration of oxalic acid (Fig. 4). In addition, it was assumed that the largest surface area is closely related to the pore volume. When oxalic acid/Na_2SiO_3 molar ratio is 15×10^{-4}, sample A2 shows the highest pore volume of 4.271 cm^3/g. The specific surface area and pore volume decreased with the agglomeration of particles because of contraction of the pore structure. Nevertheless, in case of sample A2, high pore volume was observed because of the lesser shrinkage of pores. This shrinkage was in accordance with Eq. (4), which is related to capillary stress during drying. This larger average pore diameter and the unique pore size help in reducing the drying stress. Also, sample A2 has the highest

Table 1 Physical properties of silica aerogels by varying the oxalic acid/Na_2SiO_3 molar ratios

Sample	Oxalic acid/Na_2SiO_3 molar ratio ($\times 10^{-4}$)	Specific surface area (m^2/g)	Pore volume (cc/g)	Average pore diameter (nm)	Bulk density (g/cc)	Contact angle (°)	Optical transmittance (at 550 nm)	Porosity (%)
A0	0	394	2.201	22.34	0.17	111.80	71 ± 1.5	90.5
A1	5	570.1	2.799	19.64	0.12	137.60	71 ± 2.3	93.2
A2	15	623.2	4.271	27.41	0.10	144.09	75 ± 2.1	94.3
A3	50	435.2	2.893	26.59	0.13	131.83	69 ± 1	92.7
A4	150	430.6	1.267	11.77	0.21	124.81	63 ± 1.5	88.4

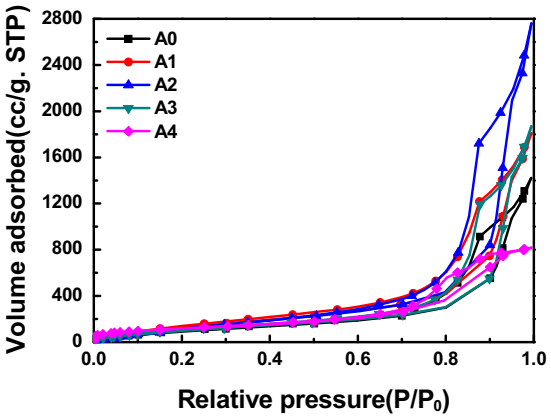

Fig. 3 Nitrogen adsorption-desorption isotherms of aerogels with variation in the oxalic acid/Na_2SiO_3 molar ratio: (A0) 0, (A1) 5×10^{-4}, (A2) 15×10^{-4}, (A3) 50×10^{-4}, and (A4) 150×10^{-4}

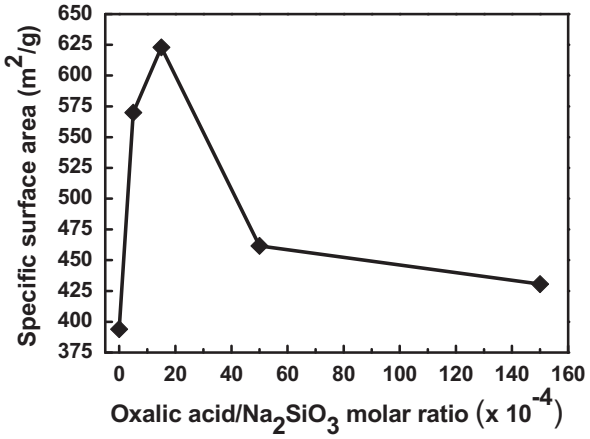

Fig. 4 Variation in specific surface area with different oxalic acid/Na_2SiO_3 molar ratios

specific surface area and the largest pore volume, as shown in Table 1.

Figure 5 shows the pore size distribution by varying the oxalic acid/Na_2SiO_3 molar ratios. It is confirmed that the addition of oxalic acid in sodium silicate solution modified the physical properties of sodium silicate-based silica aerogel, which is mainly due to the formation of a homogeneous gel and reduced shrinkage during drying. The most homogeneous pore size and the largest average pore diameter were obtained for sample A2 (Fig. 5). It can be inferred that the sample, which shows a small difference in pore size, will show less shrinkage during drying. This is also validated by the low density of sample A2 (0.10 g/cm^3). Thus, the pores of sample A2 are collapsed to a lesser extent than the other samples; this is also confirmed by the total pore volume data given in Table 1, and also when compared with the reported results by Kim et al. [28]. When the pore structure collapses, the total pore volume and the average pore size are likely to be decreased. Therefore, the

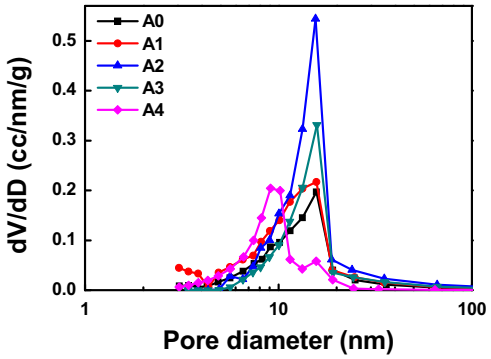

Fig. 5 Pore size distribution of aerogels based on oxalic acid/Na_2SiO_3 molar ratios: (A0) 0, (A1) 5×10^{-4}, (A2) 15×10^{-4}, (A3) 50×10^{-4}, and (A4) 150×10^{-4}

specific surface area and porosity also decrease. The excess amount of oxalic acid deteriorates the physical properties of the obtained aerogels, which can be explained by its tendency to accelerate the rate of condensation [24, 34]. The capillary pressure, caused by a difference in the pore size, is higher because of its inhomogeneous pore structure. Hence, it is affected by the volume shrinkage of the final aerogel due to the drying stress.

The microstructure of the sodium silicate-based silica aerogel by introducing oxalic acid as DCCA is shown in Fig. 6. The influence of oxalic acid as the DCCA on the microstructure of each sample can be seen in the figure. In particular, sample A2 shows a unique particle size and homogeneous pore size, but small and inhomogeneous pore structure when compared to those of the other samples. In addition, agglomeration of the particles is observed above the oxalic acid/Na_2SiO_3 molar ratio of 15×10^{-4}, as can be seen in the SEM image of sample A4 in Fig. 6. Therefore, larger clusters and particles were obtained with an inhomogeneous pore size.

Figure 7 shows the stepwise analysis of FTIR spectra of sample A2 (from gelation to the formation of final aerogel after drying). Strong Si–O–Si bonding is observed at 460 and 1100 cm^{-1} and the peak at 950 cm^{-1} exhibits Si–OH absorption, which confirms silica linkage formation [35]. Further, Si–C and C–H stretching vibrations are observed at 850, 1250, and 2900 cm^{-1}, respectively [36]. These peaks are important for understanding the differences in each step in the synthesis process. First, the peak at 2900 cm^{-1} was derived from the surface-modifying agent (Fig. 7d). However, it appears before silylation and can be explained by thermal decomposition of oxalic acid in silica wet-gel (Fig. 7a, b) [37]. Figure 8 shows the thermal decomposition reaction of oxalic acid. The decomposition of oxalic acid would occur during drying. Carbon dioxide, carbon monoxide, and water were formed after the decomposition [38]. However, the presence of residual formic acid could also be confirmed through FTIR analysis [39]. The peak at

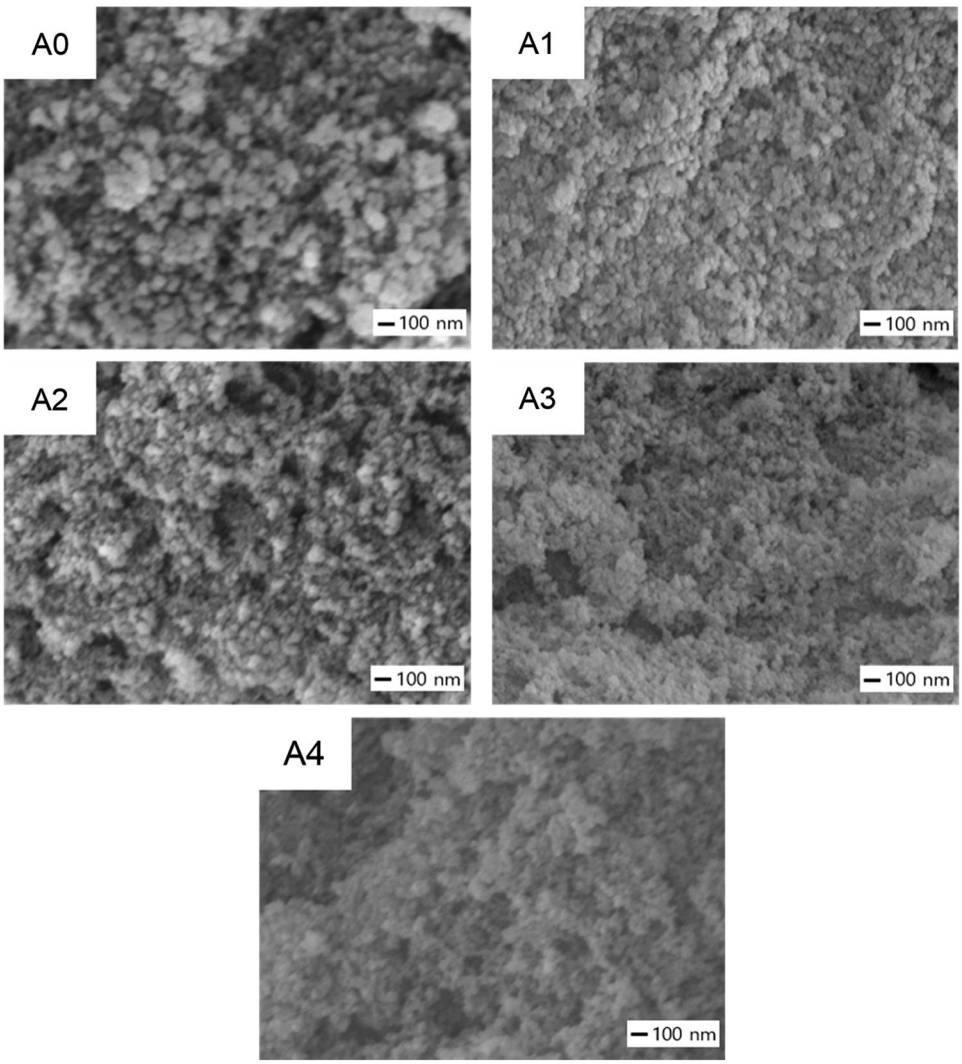

Fig. 6 SEM images of sodium silicate-based silica aerogels with different oxalic acid/Na_2SiO_3 molar ratios: (A0) 0, (A1) 5×10^{-4}, (A2) 15×10^{-4}, (A3) 50×10^{-4}, and (A4) 150×10^{-4}

2900 cm^{-1} can be attributed to C–H bonds in formic acid (Fig. 7a, b). It is important that no peaks at 850 and 1275 cm^{-1} are observed. From these absorption wavenumbers, it was confirmed that these samples show C–H bonds of formic acid instead of Si–C vibration.

In Fig. 7c, the peak at 2900 cm^{-1} for C–H bonds is not observed. In addition, it does not show the presence of Si–C bonding in the sample. It is a different phenomenon when compared to Fig. 7a, b. It was assumed that residual oxalic acid dissolved in the solvent during the aging of methanol. Although the wet-gel was washed four times with water, oxalic acid was still remained in the wet-gel due to its lower solubility in water than in methanol; the solubility of oxalic acid in water is 0.14 g/mL, while that in methanol is 0.27 g/mL [40]. It is clear from the FTIR spectrum in Fig. 7b. There was no residual oxalic acid in the silica gel or aerogel after aging in methanol, which is proved by FTIR spectra (Fig. 7c). Thus, it can be confirmed that oxalic acid affects the hydrolysis and condensation reaction. The structure of

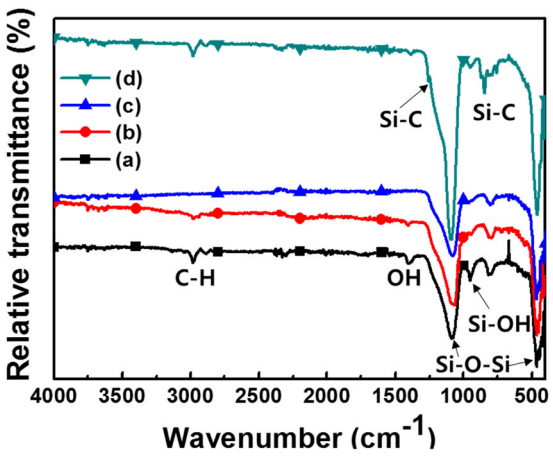

Fig. 7 FTIR spectra of dried gels at each step: **a** after gelation, **b** after washing by water, **c** after aging in methanol, and **d** final product (based on the synthesis of sample A2)

Fig. 8 Thermal decomposition reaction of oxalic acid

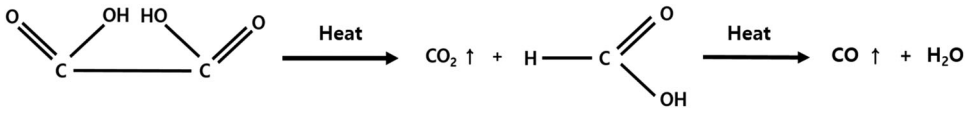

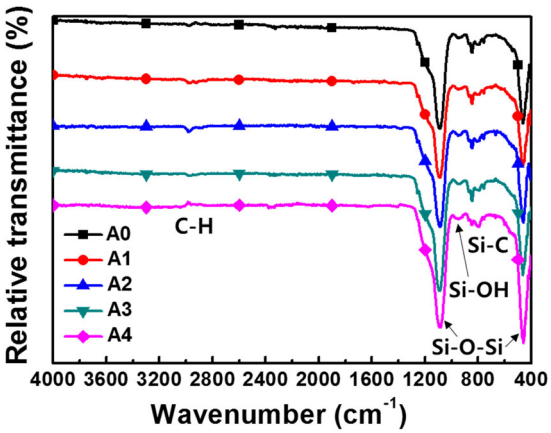

Fig. 9 FTIR spectra for aerogels with different oxalic acid/Na_2SiO_3 molar ratios: (A0) 0, (A1) 5×10^{-4}, (A2) 15×10^{-4}, (A3) 50×10^{-4}, and (A4) 150×10^{-4}

the wet-gel reflects the physical properties of the final product. Therefore, the peak at 2900 cm^{-1} after surface modification and drying appeared in Fig. 7d, which corresponds to C–H bonds in ≡Si–O–Si$(CH_3)_3$ instead of formic acid.

Figure 9 shows the FTIR spectra of sodium silicate-based silica aerogel with different oxalic acid/Na_2SiO_3 molar ratios. The primary Si–O–Si bonding at 460 and 1100 cm^{-1} shows similar absorption for each sample, as shown in Fig. 7. Furthermore, all samples showed Si–C bonding peaks at 850 and 1250 cm^{-1}, which confirms that surface modification was successful in these samples. However, the absorption of the peak at 2900 cm^{-1}, which is related to C–H bonding, is different. It is assumed that sample A2 (Fig. 9) shows a stronger absorption of C–H bonding as compared to that of the other samples. The amount of C–H bonding reflects the hydrophobicity of the sample. Therefore, the contact angle measurement is reported to validate its dependence on the absorption of C–H peak in FTIR (~2900 cm^{-1}).

The contact angle of aerogels by varying the oxalic acid/Na_2SiO_3 molar ratios is given in Table 1. The high contact angle value of ~144.09° is observed at oxalic acid/Na_2SiO_3 $= 15 \times 10^{-4}$. The hydrophilic silanol groups were transformed to hydrophobic groups by surface modification from Si–OH to Si–O–Si$(CH_3)_3$ using TMCS, which increased the hydrophobicity of the prepared aerogels. It can be assumed that oxalic acid took part in the hydrolysis and condensation of water-glass to form silanol groups, which increase with an increase in the concentration of oxalic acid. Hence, surface modification would be more hydrophobic by TMCS until oxalic acid/$Na_2SiO_3 = 15 \times 10^{-4}$. However, the contact angle decreased with increase in the molar ratio of oxalic acid/Na_2SiO_3 beyond 15×10^{-4}. This is because of the increase in the rate of condensation reaction, which leads to incomplete condensation of silanol groups [41]. In addition, the total amount of silanol groups on the surface of silica aerogel would increase with an increase in the specific surface area and the total number of silylated silanol groups is increased through surface modification. Therefore, an increase in hydrophobicity could be observed. As a result, sample A2, with the largest specific surface area, could have the highest degree of hydrophobicity. The contact angle images are shown in Fig. S1.

The optical transmittance at 550 nm is shown in Table 1. The optical transmittance at 550 nm is in the range of 63–75%, and the resultant images are given in Fig. S2. It can be confirmed that the optical transmittance varies with the molar ratio of oxalic acid/Na_2SiO_3 in sodium silicate-based silica sol. For sample A2, the highest optical transmittance of ~75% was observed. It means that the transmission of sodium silicate-based silica aerogel was enhanced by oxalic acid concentration. This effect is closely related to the homogeneity in the pore size distribution [18], shown in Fig. 5. At the molar ratio of oxalic acid/Na_2SiO_3 $= 15 \times 10^{-4}$ (Fig. 5 (A2)), narrow and uniform pore size distribution was observed, which is confirmed by the measurement of pore size distribution and described in earlier sections. On the contrary, sample A3 (Fig. 5) has less uniform pore size distribution than sample A2 (Fig. 5). In addition, sample A4 (Fig. 5) has an inhomogeneous pore size distribution. This is because of the scattering of incident light between the air and the aerogel. Hence, sample A4 has the lowest optical transmission among all samples. Optical images of all samples are given in Fig. S3.

Table 2 shows the mechanical properties of samples A0, A2, and A4 as measured by nanoindentation. Figure S4 shows the nanoindentation data for the selected three points. The elastic modulus is calculated by Eq. (5) [42]:

$$E = E_0 \times (1 - p/p_c)^f, \quad (5)$$

where E is the effective elastic modulus of porous materials with porosity p, E_0 is the elastic modulus of solid material, p_c is the porosity at which elastic modulus becomes zero, and f is the parameter dependent on the grain morphology and pore geometry of porous material. The hardness values of all the samples are similar to each other owing to their high brittleness. On the contrary, the elastic modulus, which is deeply related to the porosity of the material, decreased with an increase in the porosity of the

Table 2 Mechanical properties of sodium silicate-based aerogels

Sample	A0	A2	A4
Elastic modulus (GPa)	1.76 ± 0.326	1.56 ± 0.166	1.84 ± 0.21
Hardness (GPa)	0.12 ± 0.037	0.11 ± 0.026	0.09 ± 0.019

sodium silicate-based silica aerogel; for example, an increase from 88.4 to 94.3% was observed. In other words, brittleness increased with an increase in porosity. Sample A2 has a low elastic modulus owing to its high porosity (94.3%). However, sample A4, which has excess oxalic acid/Na_2SiO_3 molar ratio $= 15 \times 10^{-4}$, has a higher elastic modulus than sample A0, and thus low porosity (88.4%). In addition, sample A2, which has 90.5% porosity, exhibits the elastic modulus of 1.76 GPa that is a moderate value. These results are in accordance with Eq. (5). Therefore, it is confirmed that nanoindentation data are congruent with the porosity of samples A0, A2, and A4.

4 Conclusions

It was confirmed that oxalic acid can improve the physical properties of sodium silicate-based silica aerogels while acting as a DCCA with the molar ratio of oxalic acid/$Na_2SiO_3 = 15 \times 10^{-4}$. An improvement in physical properties was observed below the molar ratios of oxalic acid/$Na_2SiO_3 = 15 \times 10^{-4}$. In particular, aerogel with a molar ratio of oxalic acid/$Na_2SiO_3 = 15 \times 10^{-4}$ showed high porosity (94.3%), high specific surface area (623.2 m^2/g), high pore volume (4.271 cc/g), low density (0.10 g/cc), high optical transmittance (75%), high hydrophobicity (144.09°), and high homogeneity of pore size distribution when compared to those of other aerogels. In particular, high pore volume (4.271 g/cm^3) was derived from the narrower and uniform pore size distribution, which is related to less capillary stress on pore structure during the drying step. However, a deterioration in physical properties was observed for the samples with excess oxalic acid/Na_2SiO_3, i.e., a molar ratio of more than 15×10^{-4}. Therefore, improved physical properties could be obtained for sodium silicate-based silica aerogel at the oxalic acid/Na_2SiO_3 molar ratio $= 15 \times 10^{-4}$.

Acknowledgements This work was supported by Nano-Convergence Foundation (www.nanotech2020.org) funded by the Ministry of Science, ICT and Future Planning (MSIP, Korea) & the Ministry of Trade, Industry and Energy (MOTIE, Korea) (Project Number: R201602310).

Compliance with ethical standards

Conflict of interest The authors declare that they have no competing interests.

References

1. Dorcheh AS, Abbasi MH (2008) Silica aerogel; synthesis, properties and characterization. J Mater Process Technol 199(1–3): 10–26
2. Schmidt M, Schwertfeger F (1998) Applications for silica aerogel products. J Non Cryst Solids 225:364–368
3. Parale VG, Mahadik DB, Kavale MS, Rao AV, Wagh PV, Gupta SC (2011) Potential application of silica aerogel granules for cleanup of accidental spillage of various organic liquids. Soft Nanosci Lett 1:97–104
4. Parale VG, Lee KY, Park HH (2017) Flexible and transparent silica aerogels: an overview. J Korean Ceram Soc 54(3):184–199
5. Zhou H, Wang X, Liu H, Yan M (2017) Enhanced hydrogen storage properties of $2LiBH_4$-$LiAlH_4$ nanoconfined in resorcinol formaldehyde carbon aerogel. J Alloy Compd 726:525–531
6. Kim SJ, Jana SC (2017) Effects of skin layers on air permeability in macroporous polymer aerogels. Polymer 126:432–436
7. Haddad N, Ayadi ZB, Djessas K (2017) Synthesis and characterization of antimony doped tin oxide aerogel nanoparticles using a facile sol-gel method. J Mater Sci Mater Electron: 1–9. https://doi.org/10.1007/s10854-017-7965-4
8. Hammiche L, Slimi O, Djouadi D, Chelouche A, Touam T (2017) Effect of supercritical organic solvent on structural and optical properties of cerium doped zinc oxide aerogel nanoparticles. Optik 145:448–455
9. Sorour M, Hani HA, Al-Bazedi GA, El-Rafei AM (2016) Hydrophobic silica aerogels for oil spills clean-up, synthesis, characterization and preliminary performance evaluation. J Porous Mater 23:1401–1409
10. Shao Z, He X, Niu Z, Huang T, Cheng X, Zhang Y (2015) Ambient pressure dried shape-controllable sodium silicate based composite silica aerogel monoliths. Mater Chem Phys 162:346–353
11. Aegerter MA, Leventis N, Koebel M (2011) Aerogels handbook. Springer, New York
12. Gurav JL, Rao AV, Rao AP, Nadargi DY, Bhagat SD (2009) Physical properties of sodium silicate based aerogels prepared by single step sol-gel process dried at ambient pressure. J Alloy Compd 476(1–2):397–402
13. Bhagat SD, Kim YH, Suh KH, Ahn YS, Yeo JG, Han JH (2008) Superhydrophobic silica aerogel powders with simultaneous surface modification, solvent exchange and sodium ion removal from hydrogels. Microporous Mesoporous Mater 112(1–3):504–509
14. Bangi UKH, Kavale MS, Baek S, Park HH (2012) Synthesis of MWCNTs doped sodium silicate based aerogels by ambient pressure drying. J Sol-Gel Sci Technol 62(2):201–207
15. Bhagat SD, Kim HY, Ahn YS, Yeo JG (2006) Textural properties of ambient pressure dried water-glass based silica aerogel beads: one day synthesis. Microporous Mesoporous Mater 96(1–3): 237–244
16. Shi F, Wang L, Liu J (2006) Synthesis and characterization of silica aerogels by a novel fast ambient pressure drying process. Mater Lett 60(29–30):2718–3722
17. Rao AV, Rao AP, Kulkarni MM (2004) Influence of gel aging and Na_2SiO_3/H_2O molar ratio on monolithicity and physical properties of water-glass-based aerogels dried at atmospheric pressure. J Non Cryst Solids 350:224–229
18. Eiarsrud MA, Nilsen E, Rigacci A, Pajonk GM, Buathier S, Valette D, Durant M, Chevalier B, Nitz P, Ehrburger-Dolle F (2001) Strengthening of silica gels and aerogels by washing and aging processes. J Non Cryst Solids 285(1–3):1–7
19. Suh DJ, Park TJ, Sonn JH, Lim JC (1999) Effect of aging on the porous texture of silica aerogels prepared by NH_4OH and NH_4F catalyzed sol-gel process. J Mater Sci Lett 18:1473–1475

20. Karakuzu B, Temel TM, Yucel S, Terzioglu P, Elamis Y (2016) Effect of acid type and gelation pH on the structural properties of silica aerogels prepared by use of rice hull biosilica. Sig J Eng Nat Sci 34(2):175–182
21. Hwang SW, Kim TY, Hyun SH (2010) Effect of surface modification conditions on the synthesis of mesoporous crack-free silica aerogel monoliths from waterglass via ambient-drying. Microporous Mesoporous Mater 130(1–3):295–302
22. Mahadik DB, Jung HNR, Han W, Cho HH, Park HH (2017) Flexible, elastic, and superhydrophobic silica-polymer composite aerogels by high internal phase emulsion process. Compos Sci Technol 147:45–51
23. Cai L, Shan G (2015) Elastic silica aerogel using methyltrimethoxysilane precursor via ambient pressure drying. J Porous Mater 22:1455–1463
24. Haranath D, Rao AV, Wagh PB (1999) Influence of DCCAs on optical transmittance and porosities of TMOS silica aerogels. J Porous Mat 6(1):55–62
25. Rao AV, Kulkarni MM (2002) Effect of glycerol additive on physical properties of hydrophobic silica aerogels. Mater Chem Phys 77(3):819–825
26. He S, Cheng X, Bi H, Yang H (2014) Synthesis and effect of DCCA on the ambient pressure dried, TEOS-based silica aerogel. Adv Mater Res 1044–1045:119–123
27. Adachi T, Sakka S (1998) Sintering of silica gel derived from the alkoxysilane solution containing N,N-dimethylformamide. J Non Cryst Solids 100(1–3):250–253
28. He S, Huang D, Bi H, Li Z, Yang H, Cheng X (2015) Synthesis and characterization of silica aerogels dried under ambient pressure bed on sodium silicate. J Non Cryst Solids 410:58–64
29. Kim CE, Yoon JS, Hwang HJ (2009) Synthesis of nanoporous silica aerogel by ambient pressure drying. J Sol-Gel Sci Technol 49:47–52
30. Bangi UKH, Jung IK, Park CS, Baek S, Park HH (2013) Optically transparent silica aerogels based on sodium silicate by a two step sol-gel process and ambient pressure drying, sol-gel method. Solid State Sci 18:50–57
31. Dervin S, Lang Y, Perova T, Hinder SH, Pillai SC (2017) Graphene oxide reinforced high surface area silica aerogels. J Non Cryst Solids 465:31–38
32. Yu Y, Guo D, Fang J (2015) Synthesis of silica aerogel microspheres by a two-step acid-base sol-gel reaction with emulsification technique. J Porous Mater 22:621–628
33. Mahadik DB, Lee YK, Park CS, Chung HY, Hong MH, Jung HNR, Han W, Park HH (2015) Effect of water ethanol solvents mixture on textural and gas-sensing properties of tin oxide prepared using epoxide-assisted sol-gel process and dried at ambient pressure. Solid State Sci 50:1–8
34. He S, Zhi L, Xiaojing S, Hui Y, Lunlun G, Xudong C (2015) Rapid synthesis of sodium silicate based hydrophobic silica aerogel granules with large surface area. Adv Powder Technol 26:537–541
35. Parale VG, Mahadik DB, Mahadik SA, Kavale MS, Rao AV, Wagh PB (2012) Wettability study of surface modified silica aerogels with different silylating agents. J Sol-Gel Sci Technol 63 (3):573–579
36. Mahadik DB, Lee YK, Chavan NK, Mahadik SA, Park HH (2016) Monolithic and shrinkage-free hydrophobic silica aerogels via new rapid supercritical extraction process. J Supercrit Fluids 107:84–91
37. Higgins J, Zhou X, Liu R, Huang TTS (1997) Theoretical study of thermal decomposition mechanism of oxalic acid. J Phys Chem A 101(14):2702–2708
38. Wobbe DE, Noyes Jr. WA (1926) Photochemical studies. IV. The thermal decomposition of anhydrous oxalic acid and its relation to the photochemical decomposition. J Am Chem Soc 48:2856–2868
39. Noyes Jr WA, Wobbe DE (1926) The vapor pressure of anhydrous oxalic acid. J Am Chem Soc 48(7):1882–1887
40. Gumtya SK, Lahiri SC (2003) Ion-solvent interactions and determination of single-ion gibbs energies of transfer from the studies of the solubility and dissociation constants of oxalic acid in aquo + methanolic mixtures. Z Phys Chem 217(11):1341–1359
41. Rao AP, Pajonk GM, Rao AV (2005) Effect of preparation conditions on the physical and hydrophobic properties of two step processed ambient pressure dried silica aerogels. J Mater Sci 40 (13):3481–3489
42. Kovacik J (1999) Correlation between Young's modulus and porosity in porous materials. J Mater Sci Lett 18:1007–1010